Polar Biol (2016) 39:327–341
DOI 10.1007/s00300-015-1784-y

ORIGINAL PAPER

Distribution and vertical fluxes of silicoflagellates, ebridians, and the endoskeletal dinoflagellate *Actiniscus* in the western Arctic Ocean

Jonaotaro Onodera[1,2] · Eiji Watanabe[2] · Shigeto Nishino[2] · Naomi Harada[1,2]

Received: 16 December 2014 / Revised: 29 June 2015 / Accepted: 22 August 2015 / Published online: 14 October 2015

Abstract Spatial and temporal variations in major phytoplankton populations such as diatoms in the changing Arctic Ocean have been well studied, whereas only a few monitoring studies have been conducted on minor siliceous flagellates. To discern the relationship between hydrographic conditions and the spatio-temporal distribution of silicoflagellates, ebridians, and the endoskeletal dinoflagellate *Actiniscus pentasterias*, we analyzed seawater and bottom-tethered sediment-trap samples from the western Arctic Ocean. Silicoflagellates and ebridians were commonly observed in shelf waters around the southern Chukchi Sea in September–October during 2010 and 2013. However, one mesoscale patch with abundant silicoflagellates and ebridians was observed in the southwestern Canada Basin during September–October 2010. This offshore patch reflected an unusual occurrence of a mesoscale eddy deriving from the Alaskan Coastal Water. The active lateral transport of shelf materials by eddies was also evident in high silicoflagellate and ebridian fluxes at station Northwind Abyssal Plain (NAP) (75°N, 162°W, 1975-m water depth) in November–December during 2010 and 2011. The summer silicoflagellate flux at station NAP was mainly composed of *Distephanus speculum*. During the sea-ice cover period, except for July, silicoflagellates *D. medianoctisol* and *D. octonarius* were relatively abundant in the assemblage. The spike in *D. speculum* flux during July 2011 was observed with fecal pellets containing abundant silicoflagellates, suggesting a temporal silicoflagellate contribution to some kinds of zooplankton. The common occurrence of *A. pentasterias* in settling particles at station NAP during the winter may indicate their tolerance to cold water under sea ice.

Keywords Silicoflagellate · Ebridian · *Actiniscus pentasterias* · Sinking particles · Sediment trap · Northwind Abyssal Plain · Chukchi Sea · Arctic Ocean

Introduction

Silicoflagellates and other siliceous flagellates in sinking particles have been studied in both low- and high-latitude oceans (Takahashi 1987; Lange et al. 2000; Romero et al. 2002, 2009; Rigual-Hernández et al. 2010; Onodera and Takahashi 2012); however, few studies are reported from the Arctic Ocean (Zernova et al. 2000). In the Arctic Ocean there are snapshot records of silicoflagellate occurrences in seawater and sea ice (Melnikov 1997; Takahashi et al. 2009). Zernova et al. (2000) reported sporadic silicoflagellate occurrences in a 1-year record (from September 1995 to August 1996) of settling particle flux at station LOMO2 on the basin side of the Laptev Sea. Onodera and Takahashi (2012) considered that the relative abundance of the silicoflagellate *Distephanus medianoctisol* may increase in colder waters covered with sea ice in the Arctic Ocean compared to the subarctic North Pacific Ocean and the Bering Sea. Matsuno et al. (2014a) showed a marked relationship between the horizontal distribution of major

Electronic supplementary material The online version of this article (doi:10.1007/s00300-015-1784-y) contains supplementary material, which is available to authorized users.

✉ Jonaotaro Onodera
onoderaj@jamstec.go.jp

[1] Research and Development Center for Global Change, Japan Agency for Marine Earth Science and Technology, Natsushima-cho 2-15, Yokosuka 237-0061, Japan

[2] Institute of Arctic Climate and Environment Research, Japan Agency for Marine Earth Science and Technology, Natsushima-cho 2-15, Yokosuka 237-0061, Japan

microplankton (diatoms, dinoflagellates, and ciliates) and hydrographic differences in the western Arctic Ocean. The recent environmental changes in the western Arctic Ocean may be deciphered in the silicoflagellate assemblage. However, only limited knowledge exists regarding the modern silicoflagellate assemblage in the Arctic Ocean, except for the aforementioned reported studies. In addition, no reliable reports are present on the distribution pattern and phenology of minor siliceous flagellates such as ebridians and the endoskeletal dinoflagellate genus *Actiniscus* in the Arctic Ocean. To foster greater understanding of these siliceous flagellates in seasonal sea-ice environments, here we briefly report (1) the relationship between hydrographic variations and horizontal distributions of specific siliceous microplankton and (2) the results of a 2-year record of siliceous skeleton fluxes in the southern Northwind Abyssal Plain (NAP) in the western Arctic Ocean.

Methods

The study area included the eastern Chukchi Sea shelf and the Chukchi Borderland in the western Arctic Ocean (Fig. 1). In total, 47 water samples were collected during the R/V *Mirai* cruise MR10-05 during September–October 2010 (Fig. 1; Electric Supplementary Table 1). Additional water samples were collected during the R/V *Mirai* cruises MR12-E03 (2 samples from station NAP) on 20 September 2012 and MR13-05 (36 samples) during September–October 2013. Sea surface water was sampled by bucket, and 0.1–3.0 l was filtered through a 25- or 47-mm diameter membrane filter (0.45-μm pore size; filter area: 210 mm^2 for $\varphi = 25$ mm; 960 mm^2 for $\varphi = 47$ mm). When the ship's sampling pump was available during transit between stations on cruise MR10-05, water was pumped from an approximately 4.5 m water depth, and 2.0–6.9 l was filtered through a 47-mm-diameter membrane filter. Subsurface water from 10 to 74 m depth was collected using a conductivity-temperature-depth (CTD) Niskin bottle sampler, and water volumes of 0.3–2.0 l were filtered through a 25- or 47-mm-diameter membrane filter (Electric Supplementary Table 1). After desalting with Milli-Q water, the dried filter was cut into two pieces, and the larger piece of dried filter was mounted between a glass microscope slide and cover slip (22 × 40 mm) with Canada balsam and xylene as the resin solvent. To prepare a photomicrograph plate for studying flagellate skeletons, the remaining filter piece was used for scanning electron microscope (SEM) observation after the vapor deposition of osmium tetroxide over the filter.

Using a SMD26S-6000 type sediment trap from Nichiyu-Giken Kogyo, Co., Ltd. (Kawagoe City, Japan), the settling particle samples studied were collected at station NAP (75°N, 162°W; water-depth 1975 m) between 00:00 h on 4 October 2010 and 00:00 h on 18 September 2012. The nominal target depths were 180 m and 1300 m for the first deployment (4 October 2010–17 September 2011) and 260 and 1360 m for the second deployment (4 October 2011–8 September 2012). The sample collection bottles on the sediment traps contained filtered seawater with pH-neutralized formalin (pH ~8.2; approximate concentration, 4 %). The sampling schedule for the shallow and deep traps was the same, and the collecting interval for each sample bottle was 10–15 days (Table 1).

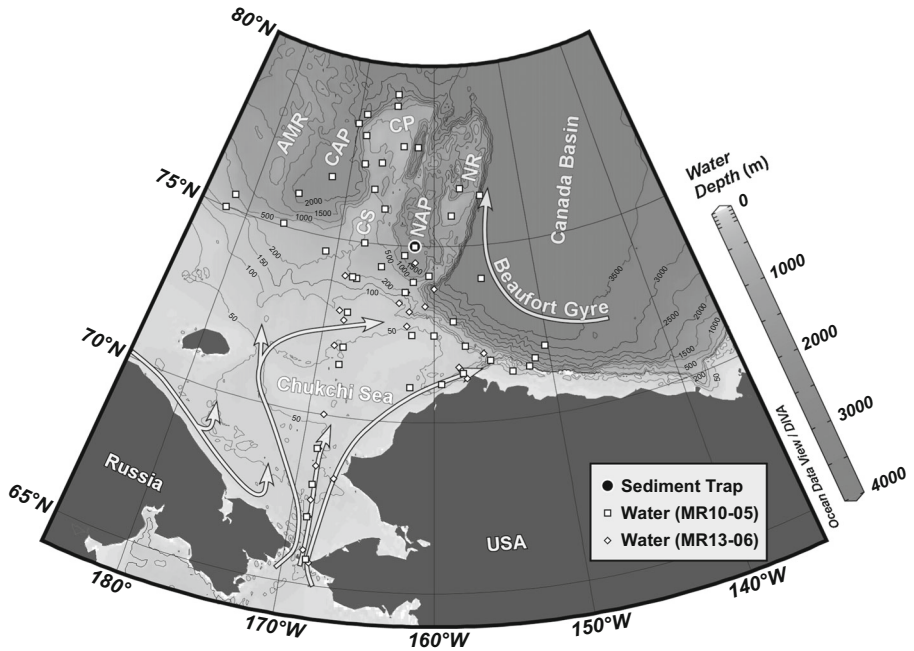

Fig. 1 Map of the study area. The *black circle* shows the location of the sediment trap mooring at station NAP. The *arrows* represent surface currents. Abbreviations of geographic areas: *NR* Northwind Ridge; *NAP* Northwind Abyssal Plain; *CS* the Chukchi Spur; *CP* Chukchi Plateau; *CAP* Chukchi Abyssal Plain; *AMR* Alpha-Mendeleev Ridge

Table 1 The sampling interval of settling particles and total mass flux at stations NAP10t and NAP11t

Deployment ID	Bottle#	Sampled date (dd mm yy)		Interval (days)	Total mass flux (mg m^{-2} d^{-1})	
		Initial	Close		Shallow	Deep
NAP10t	1	04 Oct 10	18 Oct 10	14	–	–
NAP10t	2	18 Oct 10	02 Nov 10	15	43.0	13.1
NAP10t	3	02 Nov 10	17 Nov 10	15	150.8	53.1
NAP10t	4	17 Nov 10	02 Dec 10	15	215.9	77.7
NAP10t	5	02 Dec 10	17 Dec 10	15	122.4	116.9
NAP10t	6	17 Dec 10	01 Jan 11	15	98.0	82.7
NAP10t	7	01 Jan 11	16 Jan 11	15	30.8	39.6
NAP10t	8	16 Jan 11	31 Jan 11	15	19.3	32.6
NAP10t	9	31 Jan 11	15 Feb 11	15	21.9	37.9
NAP10t	10	15 Feb 11	02 Mar 11	15	33.7	24.9
NAP10t	11	02 Mar 11	15 Mar 11	13	43.7	23.7
NAP10t	12	15 Mar 11	28 Mar 11	13	37.8	86.2
NAP10t	13	28 Mar 11	10 Apr 11	13	20.5	50.6
NAP10t	14	10 Apr 11	23 Apr 11	13	49.7	72.3
NAP10t	15	23 Apr 11	06 May 11	13	73.2	41.3
NAP10t	16	06 May 11	19 May 11	13	109.2	27.0
NAP10t	17	19 May 11	01 Jun 11	13	50.2	62.3
NAP10t	18	01 Jun 11	14 Jun 11	13	85.5	27.4
NAP10t	19	14 Jun 11	27 Jun 11	13	45.3	17.7
NAP10t	20	27 Jun 11	10 Jul 11	13	51.6	19.1
NAP10t	21	10 Jul 11	23 Jul 11	13	36.9	44.3
NAP10t	22	23 Jul 11	05 Aug 11	13	40.6	106.8
NAP10t	23	05 Aug 11	18 Aug 11	13	75.6	160.2
NAP10t	24	18 Aug 11	31 Aug 11	13	95.5	110.3
NAP10t	25	31 Aug 11	14 Sep 11	14	46.4	75.5
NAP10t	26	14 Sep 11	28 Sep 11	14	34.8	53.7
NAP11t	1	04 Oct 11	19 Oct 11	15	8.9	26.4
NAP11t	2	19 Oct 11	03 Nov 11	15	9.6	24.4
NAP11t	3	03 Nov 11	18 Nov 11	15	75.2	36.4
NAP11t	4	18 Nov 11	03 Dec 11	15	263.3	115.6
NAP11t	5	03 Dec 11	18 Dec 11	15	103.0	114.8
NAP11t	6	18 Dec 11	02 Jan 12	15	78.2	100.3
NAP11t	7	02 Jan 12	17 Jan 12	15	26.4	85.5
NAP11t	8	17 Jan 12	01 Feb 12	15	22.5	54.1
NAP11t	9	01 Feb 12	16 Feb 12	15	31.8	–
NAP11t	10	16 Feb 12	02 Mar 12	15	36.6	–
NAP11t	11	02 Mar 12	17 Mar 12	15	33.5	–
NAP11t	12	17 Mar 12	01 Apr 12	15	17.9	8.0
NAP11t	13	01 Apr 12	16 Apr 12	15	15.6	4.1
NAP11t	14	16 Apr 12	01 May 12	15	15.5	6.3
NAP11t	15	01 May 12	16 May 12	15	22.3	–
NAP11t	16	16 May 12	31 May 12	15	30.9	–
NAP11t	17	31 May 12	15 Jun 12	15	10.6	–
NAP11t	18	15 Jun 12	30 Jun 12	15	13.6	–
NAP11t	19	30 Jun 12	10 Jul 12	10	9.2	–
NAP11t	20	10 Jul 12	20 Jul 12	10	9.7	–
NAP11t	21	20 Jul 12	30 Jul 12	10	8.6	–

Table 1 continued

Deployment ID	Bottle#	Sampled date (dd mm yy)		Interval (days)	Total mass flux (mg m^{-2} d^{-1})	
		Initial	Close		Shallow	Deep
NAP11t	22	30 Jul 12	09 Aug 12	10	6.0	–
NAP11t	23	09 Aug 12	19 Aug 12	10	5.0	–
NAP11t	24	19 Aug 12	29 Aug 12	10	7.4	–
NAP11t	25	29 Aug 12	08 Sep 12	10	12.0	–
NAP11t	26	08 Sep 12	18 Sep 12	10	8.9	–

The symbol "–" indicates that assemblage analysis for this study was not conducted because of the limited sample volume

Table 2 List of study species

Taxon	References
Silicoflagellates	
Distephanus speculum (Ehrenberg) Haeckel 1887	Takahashi et al. (2009) p. 318, Pl. 2, Figs. 6–8, Pl. 3, Figs. 12–16
Distephanus medianoctisol Takahashi et al. 2009	Takahashi et al. (2009) pp. 316–318, Pl. 1, Figs. 1–11, Pl. 2, Figs. 1–5, 9–14, Pl. 3, Figs. 1–11
Distephanus octonarius (Ehrenberg) Deflandre 1932	Ling (1973) p. 752, Pl. 2, Figs. 5, 6, *Distephanus* sp. in Takahashi et al. (2009) Pl. 2, Fig. 15
Distephanus quinquangellus Bukry and Foster 1973	Bukry and Foster (1973) p. 828, pl. 5, Fig. 4; Takahashi (1987) Pl. 1, Fig. 3
Ebridian	
Ebria tripartita (Schumann) Lemmermann 1899	Vørs (1992) p. 76, Figs. 34 k–n; Osawa et al. (2005) Fig. 7a–d
Endoskeletal dinoflagellate	
Actiniscus pentasterias (Ehrenberg) Ehrenberg 1854	Orr and Conley (1976) p. 92, pl. 1, Figs. 1–11, pl. 2, Figs. 1–6

Sediment trap sample slides for light microscope observation were prepared using the methods described by Onodera et al. (2015) and as briefly summarized here. The recovered sediment trap samples were sieved through a 1-mm mesh, and the fine size fractions (<1 mm) were evenly split into the appropriate particle density for this study using a wet-sample divider (WSD-10; McLane Research Laboratories Inc., East Falmouth, MA, USA). One of the split samples was gently filtered on a membrane filter (pore size, 0.45 μm) using a vacuum pump (−0.02 MPa). The filter was desalted by rinsing it with Milli-Q water, dried in an oven (40 °C) for 1 night, and then mounted on a glass microscope slide using Canada balsam and xylene.

Skeletons on the sample slides were identified according to genus and species using a light microscope and 200–600× magnification. The morphological species taxonomy for this study is listed in Table 2. Skeleton abundance in water samples was estimated using following equation.

$$\text{Abundance}\left(\text{skeletons L}^{-1}\right) = N \times (S1/S2)/V,$$

where N is the number of counted skeletons, $S1$ is the filtered area of the sample filter (mm^2), $S2$ is the counted area (mm^2), and V is the volume of water filtered (l).

Settling skeletal fluxes were calculated using the following equation (Onodera and Takahashi 2005).

$$\text{Flux}\left(\text{skeletons m}^{-2}\text{d}^{-1}\right) = (N/S/D) \times (S1/S2) \times A,$$

where S is the aperture area of the sediment trap (0.5 m^2), D is the sampled interval (10–15 days), $S1$ is the filtered area of the sample filter (535 mm^2), $S2$ is the counted area (mm^2), and A is the aliquot size (1/100-1/1000). Skeleton abundance in water samples and calculated skeleton fluxes are listed in Electric Supplementary Tables 1 and 2. Because of the limited sample volume, deep sediment trap samples could not be analyzed from 1 February to 16 March and from 1 May to the end of deployment in 2012 (Table 1). Therefore, the results and discussion of this study are mainly based on samples from the shallower sediment traps.

Hydrographic data collected during the R/V *Mirai* cruise MR10-05 were downloaded from the JAMSTEC data search portal (http://www.godac.jamstec.go.jp/dataportal/index_eng.html). Shortwave radiation and sea-ice concentration data were obtained from the National Centers for Environmental Prediction (NCEP)/Climate Forecast System Reanalysis (CFSR) data (Saha et al. 2010). Horizontal distributions on hydrographic data and skeletal abundances

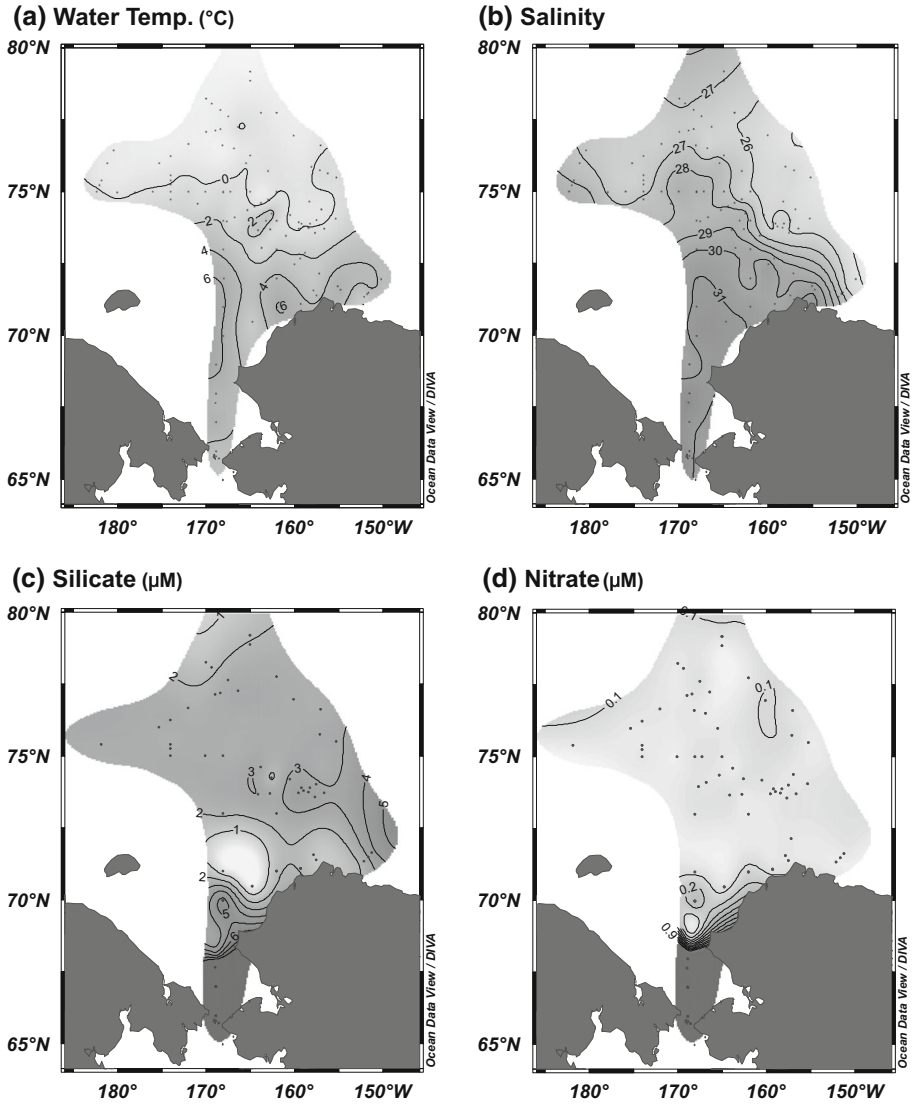

Fig. 2 Horizontal gradients of **a** water temperature (°C), **b** salinity, **c** silicate concentration (μM), and **d** nitrate concentration (μM) in the first 5 m from the sea surface of the study area during cruise MR10-05 in September–October 2010

were plotted using the Ocean Data View 4 with the DIVA interpolating method (Schlitzer 2015).

Hydrographic conditions in the study area

Surface water masses in the Chukchi Sea are categorized into Alaska Coastal Water, Bering Shelf Water, and Anadyr Water (Danielson et al. 2011). The oligotrophic water of the Beaufort Gyre covers the Canada Basin and the eastern side of the Chukchi Borderland (Nishino et al. 2011a). East Siberian Sea water appears in the western side of the Chukchi Borderland (Nishino et al. 2011a). There has been a clear decreasing trend in sea-ice extent in the Arctic Ocean since the 2000s (Stroeve et al. 2012). The sea-ice decline has influenced the intensification of the Beaufort Gyre and the nutricline deepening via the enhanced atmosphere–ocean momentum transfer (McLaughlin and Carmack 2010; Nishino et al. 2011a). The corresponding changes in water mass transport and nutrient replenishment affect marine ecosystems in the study area, such as their distribution, productivity, and extent of the sea-ice ecosystem (Grebmeier et al. 2010; Wassmann et al. 2011; Wang et al. 2013). The CTD observations during the R/V *Mirai* cruise MR10-05 showed that water temperature and salinity at around 5-m water depth ranged from −1.4 to 11.4 °C and from 24.8 to 32.5, respectively (Fig. 2a, b). During September–October 2010, an unusually large, subsurface (approximately 20–200 m depth), warm-core eddy (diameter, approximately 100 km) was found in the southwestern Canada Basin (Nishino et al. 2011b; Kawaguchi et al. 2012). This eddy was associated with the mass input of Pacific-origin Alaskan Coastal Water to the basin. The nitrate concentration in the upper water column was relatively high in the southern Chukchi Sea,

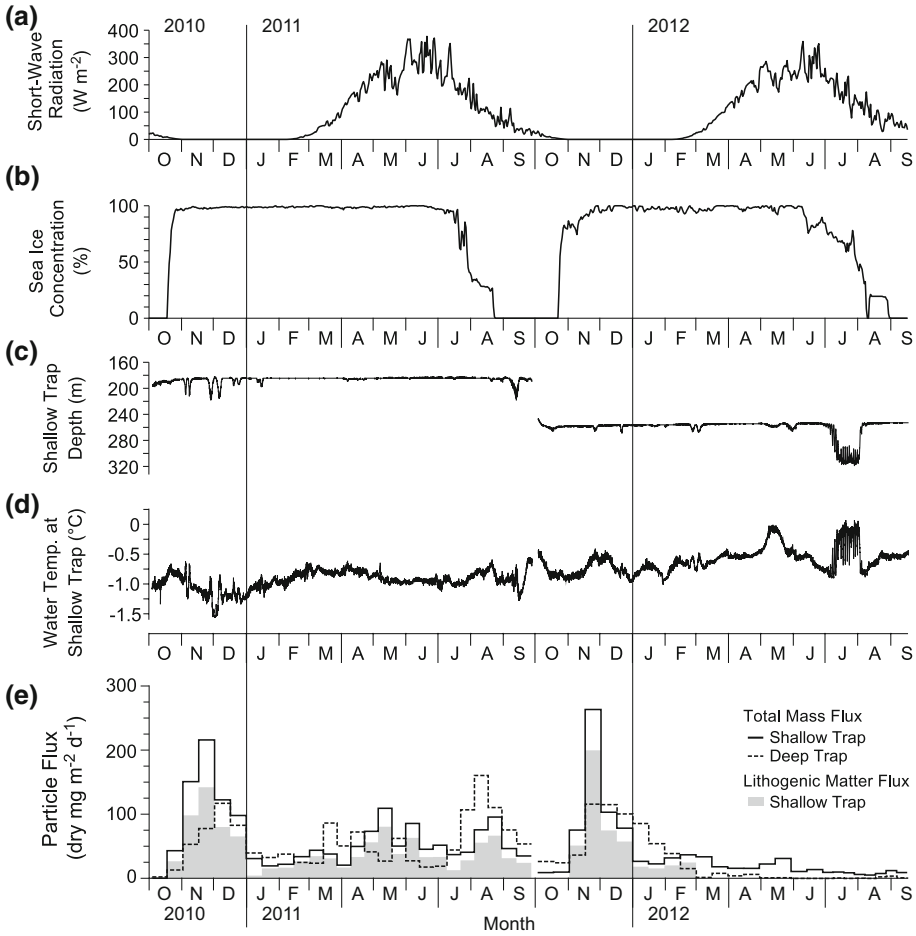

Fig. 3 Oceanographic data from station NAP obtained during the study period (4 October 2010 through 17 September 2012). **a** Short-wave radiation, **b** sea-ice concentration, **c** logged data for the depth of the moored shallow sediment trap, **d** water temperature at moored depth of the shallow sediment trap, and **e** total mass flux (<1 mm grain size) of shallow (*solid line*) and deep (*broken line*) sediment traps, and lithogenic matter flux at the shallow trap (*shaded in gray*) (Watanabe et al. 2014)

whereas it was quite low in the northern Chukchi Sea and Canada Basin during the cruise MR10-05 (September–October 2010) (Fig. 2d). The silicate concentrations in the northern Chukchi Sea were lower than those in the surrounding waters (Fig. 2c). The period of polar night at station NAP is from late October to January (Fig. 3a). Sea-ice cover was observed at station NAP from late October through late July (Fig. 3b). When the sediment traps were deployed in October 2010, the pycnocline and nutricline were observed at water depths of approximately 25 and 75 m, respectively (Fig. 4a, b).

Results

Distribution of silicoflagellate skeletons in water samples

The samples of suspended particulate matter revealed different spatial patterns for the three studied plankton groups. In surface waters (0 − ~4.5 m), common occurrence of silicoflagellate skeletons was observed in not only the southern Chukchi Sea but also over the shelf break south of station NAP during the R/V *Mirai* cruise MR10-05 during September–October 2010 (Fig. 5a). The highest skeleton density during cruise MR10-05 was 661 skeletons l^{-1} at station 6 (67°N, 168.8°W) in the southern Chukchi Sea. The mean silicoflagellate skeleton density in sea surface samples was 70 skeletons l^{-1}. The silicoflagellate skeleton abundances in the southern Chukchi Sea during cruise MR13-06 in September–October 2013 were usually higher than those during cruise MR10-05 (Fig. 6a). The maximum abundance during MR13-06 reached 39,721 skeletons l^{-1} at St. 79 (67.5°N, 168.75°W) on 4 October 2013. The high abundance of silicoflagellate skeletons observed at the shelf break and the deep sea area during cruise MR10-05 was not observed during MR13-06 (Fig. 6a).

In comparing the three sets of cruise data that include station NAP, the high subsurface abundance of silicoflagellate skeletons observed in October 2010 was not observed in September 2012 or 2013 (Fig. 4c). The subsurface maximum at station NAP was 667 skeletons l^{-1} at 75 m water depth. During cruise MR12-E03, the skeleton abundance in the subsurface chlorophyll maximum at station NAP was 112 skeletons l^{-1} (Fig. 4c). In September 2013 at station 30, which is 56 km south of station NAP,

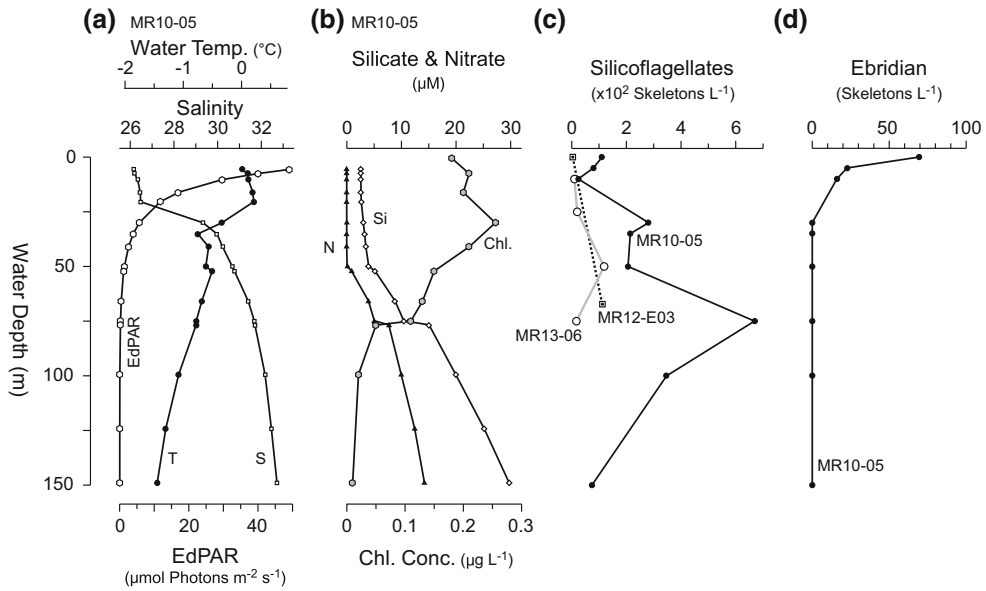

Fig. 4 Vertical hydrographic profiles for the upper 150 m of the water column at station NAP and vertical distributions of silicoflagellate and ebridian skeletons around station NAP. **a** Water temperature (°C), salinity, and downwelling irradiance of photosynthetically active radiation (EdPAR, μmol photons m^{-2} s^{-1}) on 3 October 2010; **b** silicate, nitrate, and chlorophyll concentrations (μM) on 3 September 2010 during cruise MR10-05; **c** vertical distribution of silicoflagellate skeletons ($\times 10^2$ number of skeletons l^{-1}) during the cruises MR10-05, MR12-E03, and MR13-06; **d** vertical distribution of ebridian skeletons (number of skeletons l^{-1}) on 3 September 2010 at station NAP. The data for cruise MR13-06 in **c** are from 56 km south of station NAP. There are no data in **d** for ebridians from cruises MR12-E03 or MR13-06 because their abundances were absent or were 1 skeleton l^{-1} (Electric Supplementary Table 1)

the maximum skeleton abundance through the water column was 119 skeletons l^{-1} at 50-m depth (Fig. 4c).

The dominant taxon in the study area was usually *D. speculum* (Fig. 7a, b), which is a typical cold-water species. The relative contribution of *D. medianoctisol* (Fig. 7c) and *D. octonarius* (Fig. 7d) increased to total silicoflagellates in water samples from the Canada Basin and the Chukchi Borderland (Fig. 5b).

Distribution of ebridian and *Actiniscus* skeletons in water samples

Ebridians are commonly observed in eutrophic waters around river mouths and inland seas such as the Baltic Sea and the Black Sea (Korhola and Grönlund 1999; Hargraves 2002; Osawa et al. 2005). In this study, as in previous studies of the main ebridian distribution, abundant ebridian skeletons were observed in the high-productivity area over the southern Chukchi Sea shelf rather than in the deep Canada Basin area (Figs. 5c, 6b). The ebridian distribution in the cruise MR10-05 (Fig. 5c) essentially corresponded to the sampling stations with high diatom abundance during the same cruise (Matsuno et al. 2014a). The highest skeleton density found during cruise MR10-05 was 2652 skeletons l^{-1} at station 6 (67°N, 168.8°W) in the southern Chukchi Sea. During cruise MR13-06, the highest ebridian abundance was 30,752 skeletons l^{-1} at station 79 (67.5°N, 168.75°W) in the southern Chukchi Sea on 4 October 2013. The density of ebridian skeletons over the deep Canada Basin was usually less than 50 skeletons l^{-1} at the sea surface. However, at the sea surface (0 − ~4.5 m) in September–October 2010, the area of abundant ebridians reached from Point Barrow to southwest of station NAP (Fig. 5c). At station 39 on cruise MR10-05 (74.4°N, 165.3°W), ebridian skeleton density reached 684 skeletons l^{-1}. The only ebridian species observed was *Ebria tripartita* (Table 2). At station NAP in the three cruises, common occurrence of ebridian skeletons including both living and dead specimens was only found in October 2010, and their vertical distribution was limited to the upper water column shallower than about 25-m water depth (Fig. 4d). There were almost no ebridians found around station NAP during 2012 or 2013.

The horizontal distribution of *Actiniscus pentasterias* showed the highest skeleton density of 122 skeletons l^{-1} in the Northwind Abyssal Plain (72.5°N, 162.0°W) during cruise MR10-05 (Fig. 5d). Although both ebridians and *Actiniscus* are heterotrophic flagellates, the area of high *A. pentasterias* abundance was different from that of ebridians. The latitudinal difference in density of *Actiniscus* skeletons was not large between the high-productivity area in the southern Chukchi Sea and the relatively oligotrophic Canada Basin stations during cruises MR10-05 and MR13-06 (Fig. 6c).

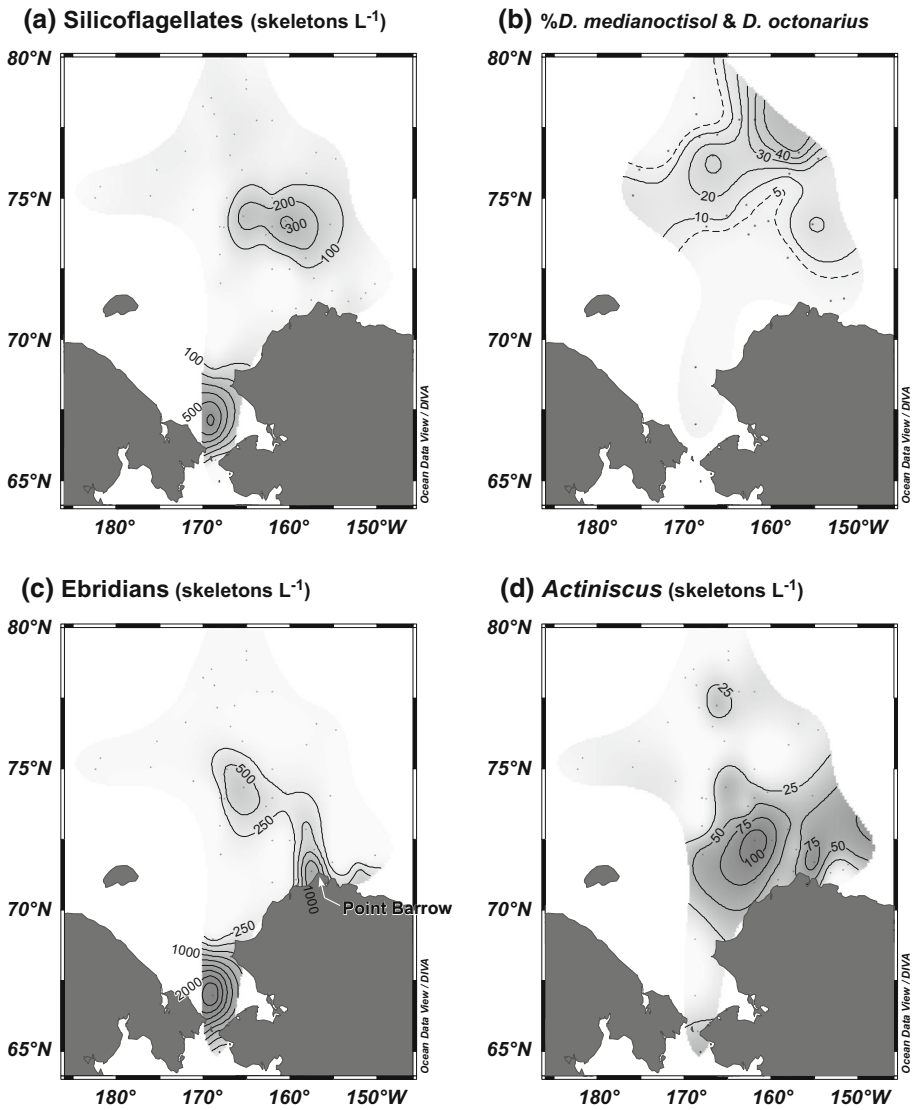

Fig. 5 Horizontal distributions of total silicoflagellates, the ebridian *Ebria tripartita*, and the endoskeletal dinoflagellate *Actiniscus pentasterias* in the sea surface waters (0 and ~4.5-m depth) during cruise MR10-05 in September–October 2010. **a** Total abundance of silicoflagellate skeletons (number of skeletons l^{-1}); **b** relative abundance (%) of *D. medianoctisol* and *D. octonarius* among total silicoflagellates (stations with fewer than 10 silicoflagellates were omitted from this *plot*); **c** abundance of ebridian skeletons (number of skeletons l^{-1}); **d** abundance of *Actiniscus pentasterias* skeletons (number of skeletons l^{-1})

Mooring depth and hydrographic conditions of shallow sediment trap

The pressure sensors mounted on the sediment traps showed that for the first deployment period (from 4 October 2010 through 27 September 2011), the deployed depths of the shallow and deep sediment traps were 181–218 (median, 185 m) and 1318–1339 m (median, 1323 m), respectively (Fig. 3c). The deployed depths for the second deployment period (from 4 October 2011 through 17 September 2012) were 247–319 (median, 256 m) and 1357–1378 m (median, 1360 m), respectively. The shallow sediment trap in the first deployment was moored in the low-temperature Pacific water layer (Matsuno et al. 2014b). A relatively rapid sinking of the upper sediment trap into the Atlantic water layer was observed during July 2012 (Fig. 3c, d). According to Matsuno et al. (2014b), the trapping efficiency for the shallow trap was within acceptable levels, except in July 2012, based on the slow current speed at station NAP in 2010 (<2.7 cm s^{-1} at 188-m water depth). Because of a substantial supply of shelf materials carried by eddies (Watanabe et al. 2014), the annual maximum of total mass flux was observed in November–December in 2010 and 2011 (Fig. 3e). According to Watanabe et al. (2014), the main bulk components of trapped particles were lithogenic materials (Fig. 3e), and the concentration of biogenic opal in the trapped samples was usually less than 20 wt%.

Flux of silicoflagellate skeletons

The settling flux of silicoflagellate skeletons at the shallow trap depth ranged from 6.9×10^3 to 288.0×10^3 skeletons m^{-2} d^{-1} throughout the sampling period (Fig. 8a). Higher fluxes were observed in November–December 2010, June–July 2011, November–December 2011, and August 2012.

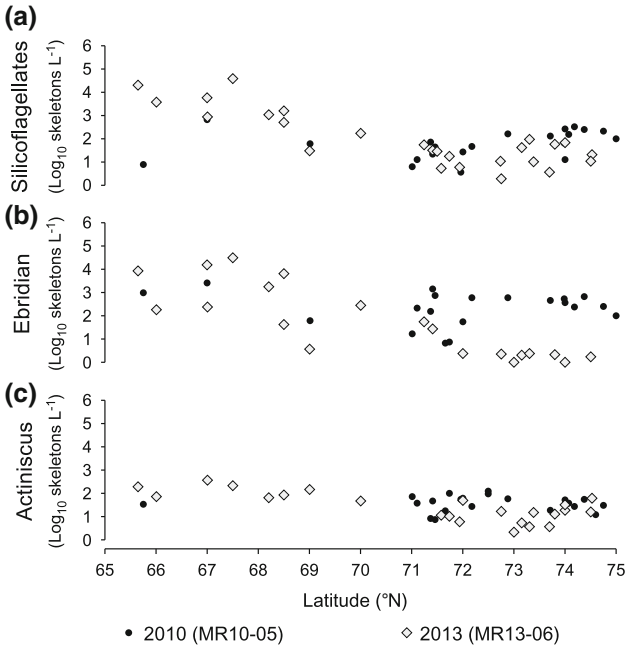

Fig. 6 Latitudinal distribution of silicoflagellate, ebridian, and *Actiniscus* skeleton abundances at the sea surface in September–October 2013 during cruise MR13-06 (*rhombic symbol* in *gray*). The data from September to October 2010 during cruise MR10-05 were plotted for comparison (*circular symbol* in *black*). Note that the *y*-axis showing skeletal abundance has a logarithmic scale

The time series fluctuation of silicoflagellate skeleton flux at the deep trap was smaller than that at the shallow trap. The settling flux of silicoflagellate skeletons at the deep trap depth ranged from 0.3×10^3 to 38.4×10^3 skeletons m^{-2} d^{-1} during the studied period except for no sample periods in 2012. In the comparison of silicoflagellate skeleton flux between shallow and deep traps in early winter, the increase of skeleton flux at the deep trap started 15–30 days later from the start of the increase in the silicoflagellate skeleton flux at the shallow trap (Fig. 8a). The summer flux maximum of silicoflagellate skeletons at the deep trap was observed in late August 2011.

Silicoflagellate fluxes were mainly composed of *D. speculum* and *D. medianoctisol* (Fig. 8b). It was characteristic of *D. medianoctisol* that the skeleton flux increases in fall to early winter compared to spring and summer. The skeletons of *D. octonarius* were rarely observed throughout the sample period. After the low flux period in winter–spring, the highest maximum of total silicoflagellate skeleton flux (288.0×10^3 skeletons m^{-2} d^{-1}) was observed at the shallow trap depth in late June–early July 2011 (Fig. 8a). Many silicoflagellate skeletons observed during this period were within pale-colored fecal pellets egested by zooplankton (Matsuno et al. 2014b, submitted) (Fig. 7f). The particle-concentrating effect of zooplankton grazing seems to be important for the occurrence of this flux maximum. In the sample with abundant pellets, silicoflagellate skeletons were commonly observed, whereas diatoms and skeletons of ebridian and *Actiniscus* were rare. The timing of the increasing silicoflagellate flux in summer 2011 was earlier than the diatom flux maximum observed during August 2011. In the periods from 1 July to 15 September of 2011 and 2012, the cumulative *D. speculum* flux in 2012 was 49 % that of the flux in 2011. In contrast, the fluxes of *D. medianoctisol* and *D. octonarius* in 2012 were 2 and 5.5 times higher than those in 2011, respectively. At seasonal time scales, the relative abundance of double skeletons (Figs. 7b, d), indicative of cells undergoing asexual reproduction, tended to be higher in summer than in winter (Fig. 8c).

For the first deployment period (345 days), the mean (±SD) silicoflagellate skeleton flux in the shallow trap was $58.6 \times 10^3 \pm 75.7 \times 10^3$ skeletons m^{-2} d^{-1}, and the median was 20.8×10^3 skeletons m^{-2} d^{-1}. For the second deployment period (350 days), the mean was $47.2 \times 10^3 \pm 38.9 \times 10^3$ skeletons m^{-2} d^{-1} and the median was 28.8×10^3 skeletons m^{-2} d^{-1}.

Flux of ebridian skeletons

The ebridian skeleton flux at the shallow trap showed annual maxima in November–December (Fig. 8d). The maximum flux was 12.0×10^3 skeletons m^{-2} d^{-1} in the shallow trap during 2–16 November 2010 (Fig. 8d). After the maximum in December, ebridian skeletons were usually absent in sediment trap samples until the following November. The flux maximum in November 2011 was approximately half of that in November 2010. All specimens collected were identified as *E. tripartita* (Fig. 7g).

Because the occurrence period of *E. tripartita* was limited, annual mean flux was close to zero. The mean daily flux of ebridian skeletons in the upper trap was $1.6 \times 10^3 \pm 3.3 \times 10^3$ skeletons m^{-2} d^{-1} for the first deployment (345 days). For the second deployment (350 days), the mean ebridian skeleton flux was $0.6 \times 10^3 \pm 1.4 \times 10^3$ skeletons m^{-2} d^{-1}.

Flux of *Actiniscus pentasterias* siliceous endoskeletons

The endoskeletal dinoflagellate *A. pentasterias* was observed in all sediment trap samples (Fig. 8d). The maximum flux was 22.0×10^3 skeletons m^{-2} d^{-1} in the shallow trap over the interval from 17 November to 1 December 2010. The flux was relatively high in early winter to late spring and was low in summer (Fig. 8d). Some skeletons were relatively large in size (maximum diameter, 40.5 μm; mean, 21.5 ± 4.6 μm; $n = 66$ from the first deployment). Skeletons reaching 40 μm in diameter have not been observed at station SA in the northern subarctic North Pacific (maximum diameter, 30.4 μm; mean, 22.0 ± 3.9 μm; $n = 105$; Onodera unpublished data).

The mean daily flux of *Actiniscus* skeletons in the upper trap for the first deployment (345 days) was $9.8 \times 10^3 \pm 6.3 \times 10^3$ skeletons m^{-2} d^{-1}. For the second deployment (350 days) the mean was $5.9 \times 10^3 \pm 3.8 \times 10^3$ skeletons m^{-2} d^{-1}.

Discussion

The comparison of skeletal fluxes in the Arctic Ocean and Bering Sea

The silicoflagellate flux at station LOMO2 in the area of seasonal sea ice (81°04.3′N, 138°55.2′E, 1730-m water depth, 150-m trap depth) ranged from 1.3×10^3 to 10.2×10^3 skeletons m^{-2} d^{-1} from 15 September 1995 through 16 August 1996 (Zernova et al. 2000). The maximum skeletal flux at station NAP was higher than that at station LOMO2. The mean silicoflagellate flux in our study was one order of magnitude lower than those in previous studies of silicoflagellate skeletal fluxes in the Bering Sea (Onodera and Takahashi 2012) and the eastern subarctic North Pacific (Takahashi 1987). At station AB in the southern Bering Sea in 1990–1994, *D. medianoctisol* had a mean relative abundance of 4 %, and *D. octonarius* was absent (Onodera and Takahashi 2012). The mean relative abundances of *D. medianoctisol* and *D. octonarius* were

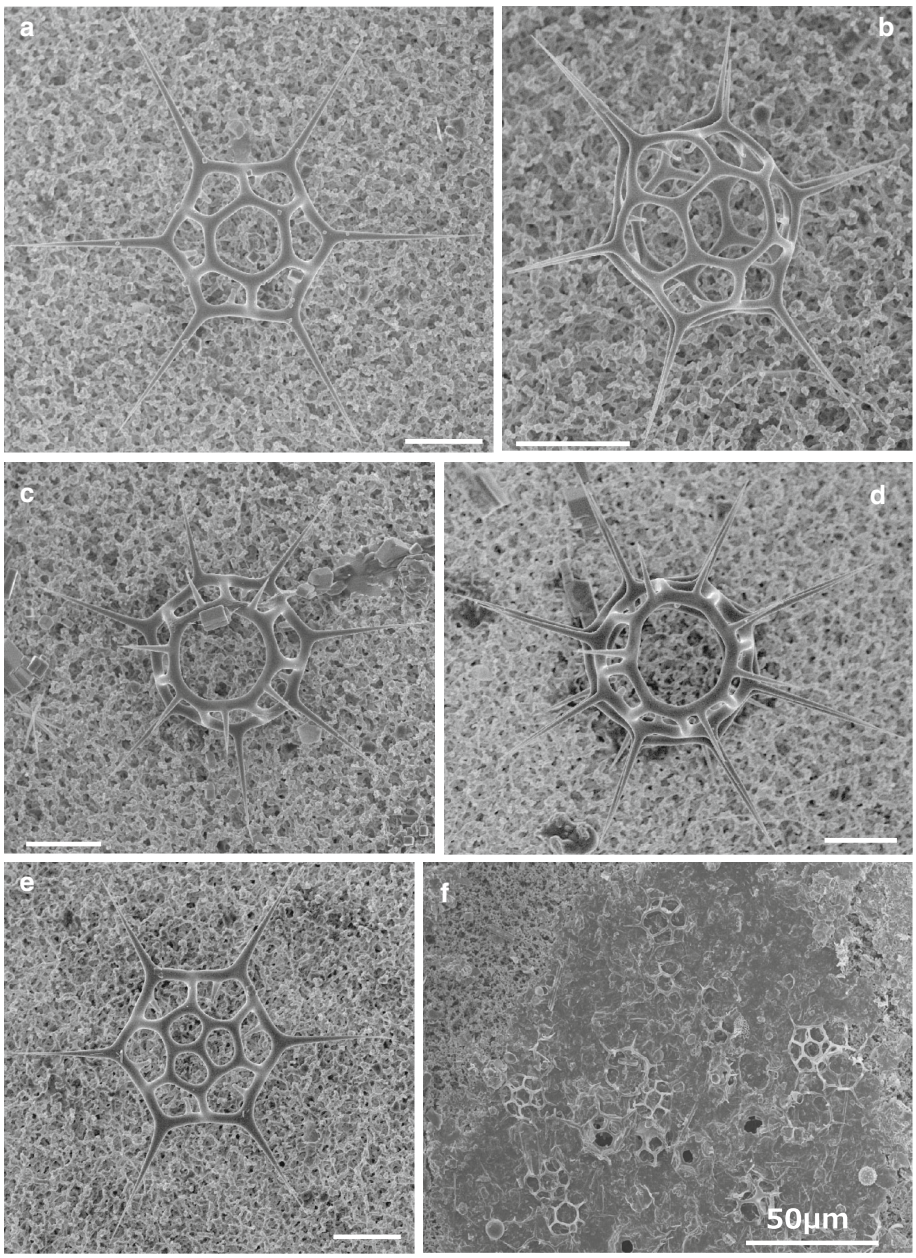

Fig. 7 Photomicrographs of silicoflagellate, ebridian, and *Actiniscus pentasterias* skeletons from the western Arctic Ocean. *Scale bars* 10 µm, except for **f**. **a** *Distephanus speculum*; **b** double skeleton of *D. speculum*; **c** *D. medianoctisol*; **d** double skeleton of *D. octonarius*; **e** *Distephanus speculum,* s.l. (this specimen is similar to *D. boliviensis* var. *major*, but differs from typical *D. boliviensis major* in the smaller skeleton and the absence of an apical spine); **f** aggregated particle containing abundant silicoflagellate skeletons; **g**, **h** ebridian *Ebria tripartita*; **i**–**l** endoskeletal dinoflagellate *Actiniscus pentasterias*. The specimens in images **a**–**e** were obtained during the R/V *Mirai* cruise MR10-05 at station 126 (sampled water depths: **a** 75 m, **b**, **d**, **e** 50 m, and **c** 35 m). The specimen in **f** was taken from the shallow sediment trap sample from 27 June to 10 July 2011. Images **g**–**j** show specimens from the ship's seawater pump system obtained at 74°N, 162°W during cruise MR10-05 on 27 September 2010

Fig. 7 continued

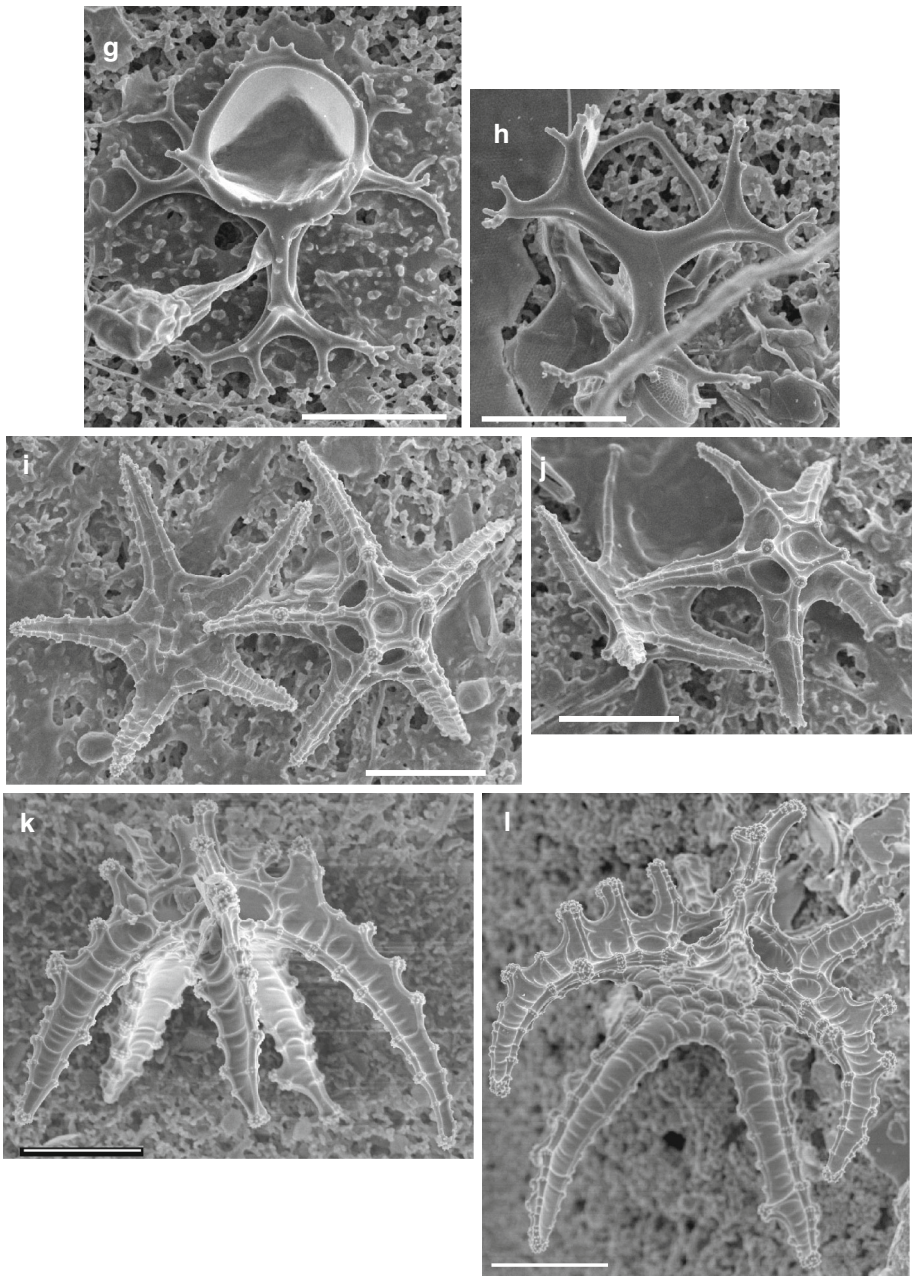

26.3 and 2.3 % at the shallow trap at station NAP for the studied period.

The mean ebridian flux at station NAP was two orders of magnitude lower than that at station AB (53.5°N, 177°W, 3200-m trap depth, 3788-m water depth) in the Aleutian Basin of the Bering Sea for August 1990–July 1994 (14.7×10^3 skeletons m^{-2} d^{-1}; Onodera and Takahashi unpublished data). Hargraves (2002) reported that *E. tripartita* favors preying on diatoms compared to dinoflagellates. The lower daily mean of diatom flux at station NAP (1.9×10^6 valves m^{-2} d^{-1}; Onodera et al. 2015) than at station AB (52.6×10^6 valves m^{-2} d^{-1} for 1990–1998; Onodera and Takahashi 2012) might be related to the lower ebridian flux at station NAP. The sinking flux of *A. pentasterias* skeletons in this study was one order of magnitude lower than that at station AB in the southern Bering Sea for 1990–1994 (mean, 29.6×10^3 skeletons m^{-2} d^{-1}; median, 25.2×10^3 skeletons m^{-2} d^{-1}; Onodera and Takahashi unpublished data) and in the eastern subarctic North Pacific (Takahashi 1987).

Silicoflagellates in sea-ice flora

The silicoflagellate assemblages in the sea-ice-covered environments of the study area were characterized by the common occurrence of *D. medianoctisol* and the rare

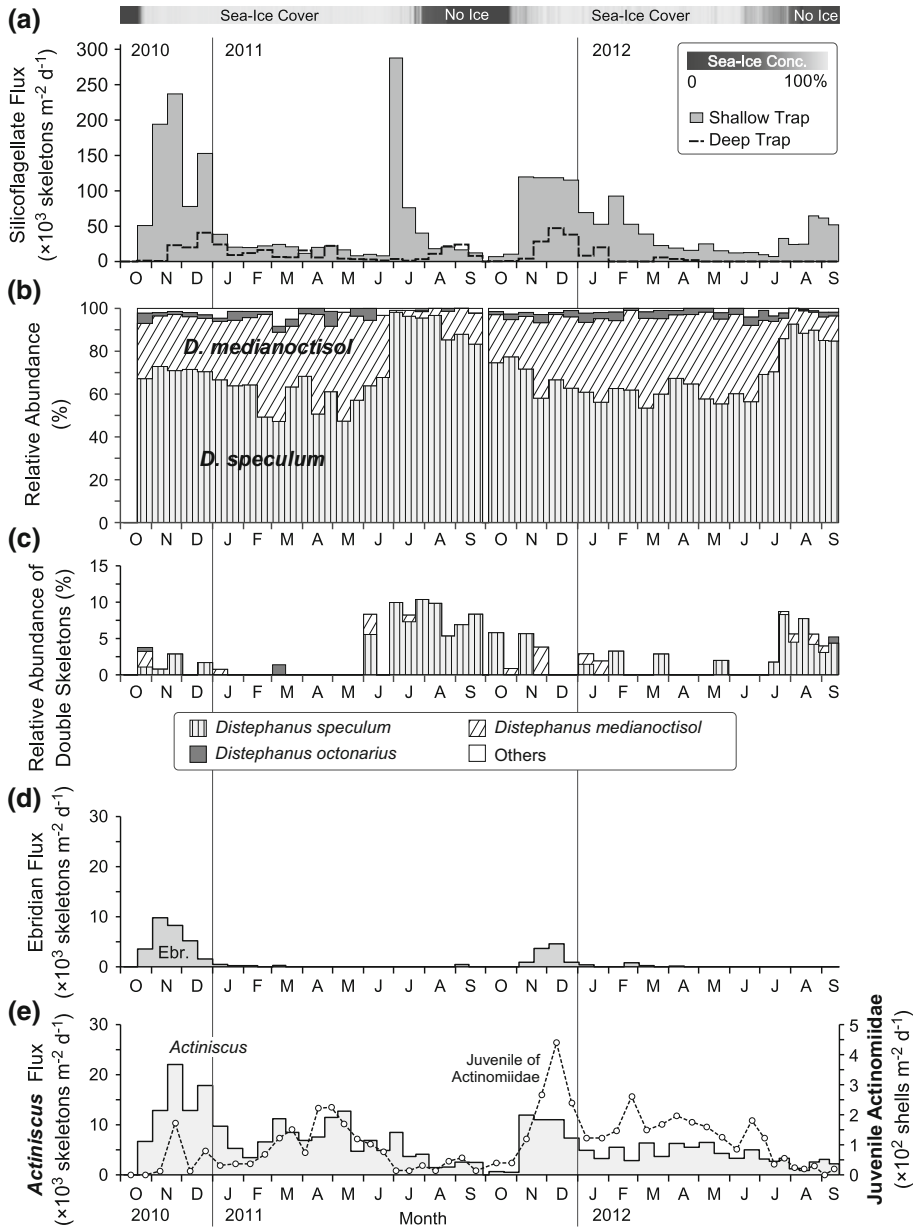

Fig. 8 Time series of settling fluxes of siliceous flagellate skeletons at station NAP from 4 October 2010 to 18 September 2012. **a** Silicoflagellate skeleton flux at shallow and deep trap depths. There are no deep trap data for 4–18 October 2010 or for 1 February–16 March and 1 May–18 September 2012. **b** Relative abundances in silicoflagellate skeleton assemblage, **c** relative abundance of double skeletons among total silicoflagellate skeletons, **d** skeleton fluxes of ebridian, and **e** skeleton fluxes of the endoskeletal dinoflagellate *Actiniscus* and the juvenile form of radiolarian Actinomiidae (Ikenoue et al. 2015) in the shallow sediment trap samples. The category named "others" in Fig. 8b, c is composed of *D. quinquangellus* and unidentified aberrant skeletons

occurrence of *D. octonarius*. In general, these species are absent or very rare in the subarctic and lower latitude oceans (Malinverno 2010; Onodera and Takahashi 2012). In previous records of silicoflagellate skeletons in the Arctic Ocean, *D. speculum* and *D. medianoctisol* were reported from plankton assemblages, whereas *D. medianoctisol* and *D. octonarius* have been categorized as sea-ice flora (Melnikov 1997). *Distephanus* skeletons with seven and eight sides were observed in high abundance in a pancake-ice environment of the Southern Ocean (78°10′S, 162°W; Haeckel 1887). In the modern Southern Ocean, the relative abundance of heptagonal skeletons increases at higher latitudes with sea surface temperatures less than −1 °C (Malinverno 2010). *Distephanus medianoctisol* was dominant in the silicoflagellate flora of seawater, in the diatom mat under sea ice, and within sea ice over the northern Lomonosov Ridge near the North Pole in August–September 2004 (Takahashi et al. 2009). During cruise MR10-05, *D. medianoctisol* and *D. octonarius* had higher relative abundances in waters with lower salinity and lower temperature (Figs. 2, 5b). These observations suggest that the flux increase of *D. medianoctisol* in the early winter corresponds to the colder water conditions during sea-ice formation. However, it is not clear why *D. speculum* instead of *D. medianoctisol* dominated the silicoflagellate assemblage under sea ice in July 2011. According to the biogeography of silicoflagellate skeletons at surface sediments in the North Pacific (Poelchau 1976), the relative

abundance of *D. speculum* tends to be higher along the coast of subarctic North Pacific and the Bering Sea. This distribution pattern of *D. speculum* may suggest their character as a mesotrophic-eutrophic species in cold waters. Arrigo et al. (2012) reported the under-ice bloom was mainly composed of planktic diatoms instead of ice algae over the northern Chukchi Sea in July 2011. If dominance of *D. speculum* reflects a high nutrient availability, favorable nutrient and light conditions in the subsurface under sea ice might support the active production and dominance of *D. speculum* at station NAP in July 2011.

Different seasonality in *Actiniscus* and ebridian fluxes

Because *A. pentasterias* and ebridian are heterotrophic flagellates, their high abundance is supported by abundant biological production. The fluxes of *A. pentasterias* skeletons in the eastern North Pacific show a significant correlation with total mass fluxes (Takahashi 1987). A significant correlation existed between *Actiniscus* skeletal flux and total mass flux in this study ($r = 0.72$, $p < 0.01$) for the entire study period. However, the major bulk component of sinking particles was silt-clay minerals (Fig. 3e); the correlation between *A. pentasterias* flux and POC flux was insignificant ($r = 0.21$, $p = 0.24$). In the comparison of sinking microplankton fluxes, the time series variation of *A. pentasterias* flux at station NAP was similar to the time series fluxes of radiolarian species (juvenile of Actinommidae spp., Ikenoue et al. 2015) in the same samples except for the early winter in 2010 (Fig. 8e). In the study area, the juvenile of Actinommidae spp. dwells in the euphotic layer, and this taxon shows tolerance to cold water under sea ice (Ikenoue et al. 2015). The time series fluctuation in sinking fluxes of *Actiniscus* suggests a similar tolerance to cold water under sea ice. In September–October 2010, *E. tripartita* and diatom cells were frequently observed in sea surface waters along the shelf break of the northern Chukchi Sea north of Point Barrow (Figs. 5c, and 2a in Matsuno et al. 2014a). The water with abundant diatoms in the cruise MR10-05 corresponded the Pacific-origin coastal water with higher temperature, salinity and nutrients (Matsuno et al. 2014a). However, the ebridian sinking flux did not increase during spring–summer even in the period of high diatom production as ebridian's food source at station NAP. It seems that the temporal advection of shelf waters into the southwestern Canada Basin and Chukchi Borderland was the main reason for the limited occurrence period of ebridian in the sinking particles at station NAP in the early winter.

Lateral input of Pacific-origin shelf waters

The mesoscale patchy distribution of abundant silicoflagellates at the sea surface in the northern Chukchi Sea in September–October 2010 (Fig. 5a) corresponded to the location of a large anti-cyclonic warm-core eddy (about 100-km diameter) (Nishino et al. 2011b; Kawaguchi et al. 2012). The eddy-like signal was slightly vague in the sea surface temperature shown in Fig. 2a. However, the vertical profile clearly captured the main body of the warm-core eddy located below 20 m depth. The readers can see the detailed eddy property obtained from the same cruise (Nishino et al. 2011b; Kawaguchi et al. 2012). Nitrate concentrations in the northern Chukchi Sea and Canada Basin are usually very low in summer (Fig. 2d). However, the observed warm-core eddy transported large amounts of ammonium from the Chukchi Sea shelf to the subsurface layers near the euphotic zone in the western Canada Basin, and this lateral nutrient advection supported the primary producers, mainly composed of pico-phytoplankton, around the eddy (Nishino et al. 2011b). This effect might be observed in the microplankton assemblages along with the warm core eddy. In general, an eddy-like chlorophyll feature is evident in ocean color satellite images of the study area, and a hot spot of high primary production caused by eddy-induced vertical mixing was demonstrated by the western Arctic marine ecosystem model (Watanabe et al. 2012). However, the direct observation of an unusual large warm-core eddy during the cruise MR10-05 in October 2010 suggests that the unusual offshore patch of abundant silicoflagellates in September–October 2010 can be explained by the eddy-induced advection of Pacific-origin shelf waters to the southwestern Canada Basin rather than an upwelled nutrient supply from the subsurface of Canada Basin.

These observations of water samples and hydrography in the study area suggest that the high settling fluxes of studied siliceous flagellates and clay minerals at station NAP in October–December of 2010 and 2011 (Figs. 3e, 8) reflect the several origins of settling particles from autochthonous microplanktons around station NAP and the lateral inputs of shelf materials into the deep Canada Basin. In late summer–early winter, juvenile bivalves that are observed in shelf waters were also observed in the sediment trap samples (Watanabe et al. 2014). The occurrence of juvenile bivalves at station NAP is one piece of biological evidence for the lateral input of shelf materials to the Canada Basin. As with the juvenile bivalves, some of the *E. tripartita* observed in this study might have come from the Chukchi Sea shelf. According to a physical oceanographic simulation (Watanabe et al. 2014) using the sea ice-ocean general circulation model COCO 4.9 (Hasumi 2006), a substantial amount of shelf water can be transported to areas offshore, including to

the station NAP in November, by a cold eddy generated off Point Barrow during May–June. Watanabe et al. (2014) suggested that the generation mechanism and location of this cold eddy and the aforementioned warm eddy were basically the same, and the arising period was, however, different off Point Barrow (cold eddy in May–June; warm eddy after July). The lateral advection of the cold eddy is observed in the subsurface around 100–200 m depth in the study area (Watanabe et al. 2014). Therefore, the eddy formation and westward advection along the shelf break or oceanic Beaufort Gyre take an important role for the temporal increase of shelf materials including coastal microplanktons such as ebridian in sinking particles at station NAP. Active circulation is evident at the sea surface when sea ice retreats to the north, and winds directly influence the physical oceanographic conditions at the sea surface. In summer 2013, sea ice remained around station NAP. In this situation, the ebridians were concentrated in the southern Chukchi Sea, whereas their abundance was low in the northern Chukchi Sea and Chukchi Borderland (Fig. 6b). It is expected that the time series variation of ebridian flux at station NAP in 2013 may be different from those in 2010–2012, although the analysis of the sediment trap samples from October 2012 to September 2014 has not been started at this time (Fig. 8d). To understand the interannual variation in the relationship between microplankton assemblages and hydrography, time series monitoring around the Chukchi Sea and southwestern Canada Basin is in progress.

Contribution of silicoflagellates to lower trophic ecosystems

The spike in the flux of silicoflagellate skeletons and presence of fecal pellets containing many silicoflagellate skeletons (Fig. 7f) in June–July 2011 suggest a substantial silicoflagellate contribution to microzooplankton production under the sea ice around station NAP. Diatom valves were rare in the fecal pellets with many silicoflagellate skeletons. According to Matsuno et al. (submitted), vertical fluxes of mesozooplankton fecal pellets increased in the same samples showing the silicoflagellate flux maximum in June–July 2011. The relative increase of silicoflagellate double skeletons in summer (Fig. 8c) may support the active silicoflagellate production (Takahashi et al. 1990). On the basis of the mean skeleton size of 52 specimens of *D. speculum* and the equation for converting cell size to carbon content (Menden-Deuer and Lessard 2000), we estimated that silicoflagellate carbon accounted for 2.6 % of the total POC flux in June–July 2011. The silicoflagellate contribution to POC flux is usually low (e.g., Takahashi et al. 1990). In this study, the *D. speculum* contribution to POC flux ranged from 0.05 to 0.98 %, except for late June–July 2011. Therefore, as found in previous studies, the silicoflagellate contribution to POC flux is usually minor. However, silicoflagellates in the sea-ice environment in the continental shelf of Southern Ocean may make a substantial contribution to food webs (Fragoso and Smith 2012). In the Arctic Ocean, high silicoflagellate abundance has been reported in the summer sea-ice flora around the North Pole in 2004 (Takahashi et al. 2009). Because the increase in fluxes of diatom valves at station NAP began in August 2011 (Onodera et al. 2015), the silicoflagellate flux maximum in late June–July 2011 suggests that silicoflagellates could be a food source for some kinds of micro- and meso-zooplankton at certain times.

Acknowledgments We are grateful for the excellent assistance with the mooring operations provided by the captains, crew, chief scientists, onboard technician, and scientists of the R/V *Mirai* [Japan Agency for Marine Earth Science and Technology (JAMSTEC)] cruises MR10-05, MR12-E03 and MR13-06, and I/B CCGS *S. W. Laurier* in 2011. We thank Dr. Takashi Kikuchi (JAMSTEC) for cruise logistics, and Dr. Yuichiro Tanaka [National Institute of Advanced Industrial Science and Technology (AIST), Japan] for providing the sediment trap equipment. This work was funded by a Grant-in-Aid for Scientific Research (S) of the Japan Society for the Promotion of Science (JSPS) JFY2010-2014, no. 22221003, "Catastrophic reduction of sea ice in the Arctic Ocean: its impact on the marine ecosystems in the polar region" to N.H., a Grant-in-Aid for Scientific Research (A) of JSPS, no. 15H01736, and JSPS Research Fellowships for Young Scientists no. 22-5808 to J.O.

References

Arrigo KR, Perovich DK, Pickart RS, Brown ZW, van Dijken GL, Lowry KE, Mills MM, Palmer MA, Balch WM, Bahr F, Bates NR, Benitez-Nelson C, Bowler B, Brownlee E, Ehn JK, Frey KE, Garley R, Laney SR, Lubelczyk L, Mathis J, Matsuoka A, Mitchell BG, Moore WK, Ortega-Retuerta E, Pal S, Polashenski CM, Reynolds RA, Schieber B, Sosik HM, Stephens M, Swift JH (2012) Massive phytoplankton blooms under Arctic Sea ice. Science 336:1408

Bukry D, Foster JH (1973) Silicoflagellate and diatom stratigraphy, Leg 16, Deep Sea Drilling Project. In: Van Andel TH, Heath GR et al (eds) Initial Rep DSDP 16:815–871

Danielson S, Curchitser E, Hedstrom K, Weingartner T, Stabeno P (2011) On ocean and sea ice modes of variability in the Bering Sea. J Geophys Res 116:C12034. doi:10.1029/2011JC007389

Deflandre G (1932) Sur la systématique des Silicoflagellés. Bull Soc Bot France 79:494–506

Ehrenberg CG (1854) Mikrogeologie. Leopold Voss, Lipzig

Fragoso GM, Smith WO Jr (2012) Influence of hydrography on phytoplankton distribution in the Amundsen and Ross Seas, Antarctica. J Mar Syst 89:19–29

Grebmeier JM, Moore SE, Overland JE, Frey KE, Gradinger R (2010) Biological response to recent Pacific Arctic Sea ice retreats. Eos 91:161–162

Haeckel E (1887) Report on the radiolaria collected by H.M.S. Challenger during the years 1873–1876. Report on the scientific results of the voyage of H.M.S. Challenger during the years 1873–1876 18:1–1803

Hargraves PE (2002) The ebridian flagellates *Ebria* and *Hermesinum*. Plankton Biol Ecol 49:9–16

Hasumi H (2006) CCSR ocean component model (COCO) version 40, Center for Climate System Research Report, vol 25. University of Tokyo, Tokyo, pp 1–103

Ikenoue T, Bjørklund KR, Krugulikova SB, Onodera J, Kimoto K, Harada N (2015) Flux variations and vertical distributions of siliceous Rhizaria (Radiolaria and Phaeodaria) in the western Arctic Ocean: indices of environmental changes. Biogeosciences 12:2019–2046

Kawaguchi Y, Itoh M, Nishino S (2012) Detailed survey of a large baroclinic eddy with extremely high temperatures in the Western Canada Basin. Deep Sea Res I 66:90–102

Korhola A, Grönlund T (1999) Observations of *Ebria tripartita* (Schumann) Lemmermann in Baltic sediments. J Paleolimnol 21:1–8

Lange CB, Weinheimer AL, Reid FMH, Tappa E, Thunell RC (2000) Response of siliceous microplankton from the Santa Barbara Basin to the 1997–1998 El Nino event. Cal Coop Ocean Fish 41:186–193

Lemmermann E (1899) Ergebnisse einer Reise nach dem Pacific. Planktonalgen Abh. Naturwiss. Ver. Bremen 16:313–398

Ling HY (1973) Silicoflagellates and ebridians from leg 19. In: Creager JS, Scholl DW et al (eds) Initial Rep DSDP 19:751–775

Malinverno E (2010) Extant morphotypes of *Distephanus speculum* (Silicoflagellata) from the Australian sector of the Southern Ocean: morphology, morphometry and biogeography. Mar Micropaleontol 77:154–174

Matsuno K, Ichinomiya M, Yamaguchi A, Imai I, Kikuchi T (2014a) Horizontal distribution of microprotisst community structure in the western Arctic Ocean during late summer and early fall of 2010. Polar Biol 37:1185–1195

Matsuno K, Yamaguchi A, Fujiwara A, Onodera J, Watanabe E, Imai I, Chiba S, Harada N, Kikuchi T (2014b) Seasonal changes in mesozooplankton swimmers collected by sediment trap moored at a single station on the Northwind Abyssal Plain in the western Arctic Ocean. J Plankton Res 36:490–502

Matsuno K, Yamaguchi A, Fujiwara A, Onodera J, Watanabe E, Harada N, Kikuchi T (submitted) Seasonal changes in meso zooplankton swimmer community and faecal pellets collected by sediment trap moored at the Northwind Abyssal Plain in the western Arctic Ocean. Polar Biol

McLaughlin FA, Carmack EC (2010) Deepening of the nutricline and chlorophyll maximum in the Canada Basin interior, 2003–2009. Geophys Res Lett 37:L24602. doi:10.1029/2010GL045459

Melnikov IA (1997) The Arctic sea ice ecosystem. Gordon and Breach Science Publishers, Amsterdam

Menden-Deuer S, Lessard EJ (2000) Carbon to volume relationships for dinoflagellates, diatoms, and other protist plankton. Limnol Oceanogr 45:569–579

Nishino S, Kikuchi T, Yamamoto-Kawai M, Kawaguchi Y, Hirawake T, Itoh M (2011a) Enhancement/reduction of biological pump depends on ocean circulation in the sea-ice reduction regions of the Arctic Ocean. J Oceanogr 67:305–314

Nishino S, Itoh M, Kawaguchi Y, Kikuchi T, Aoyama M (2011b) Impact of and unusually large warm-core eddy on distributions of nutrients and phytoplankton in the southwestern Canada Basin during late summer/early fall 2010. Geophys Res Lett 38:L16602. doi:10.1029/2011GL047885

Onodera J, Takahashi K (2005) Silicoflagellate fluxes and environmental variations in the northwestern North Pacific during December 1997–May 2000. Deep Sea Res I 52:371–388

Onodera J, Takahashi K (2012) Oceanographic conditions influencing silicoflagellate flux assemblages in the Bering Sea and subarctic Pacific Ocean during 1990–1994. Deep Sea Res II 61–64:4–16

Onodera J, Watanabe E, Harada N, Honda MC (2015) Diatom flux reflects water-mass conditions on the southern Northwind Abyssal Plain, Arctic Ocean. Biogeosciences 12:1373–1385. doi:10.5194/bg-12-1373-2015

Orr WN, Conley S (1976) Siliceous dinoflagellates in the northeast Pacific rim. Micropaleontology 22:92–99

Osawa M, Takahashi K, Hay BJ (2005) Shell-bearing plankton fluxes in the central Black sea, 1989–1991. Deep Sea Res I 52: 1677–1698

Poelchau HS (1976) Distribution of Holocene silicoflagellates in North Pacific sediments. Micropaleontology 22:164–193

Rigual-Hernández AS, Bárcena MA, Sierro FJ, Flores JA, Hernandz-Almeida H, Sanchez-Vidal A, Palanques A, Heussner S (2010) Seasonal to interannual variability and geographic disribuiton of the silicoflagellate fluxes in the Western Mediterranean. Mar Micropaleontol 77:46–57

Romero O, Lange CB, Wefer G (2002) Interannual variability (1988–1991) of siliceous phytoplankton fluxes off northwest Africa. J Plankton Res 24:1035–1046

Romero O, Rixen T, Herunadi B (2009) Effects of hydrographic and climatic forcing on diatom production and export in the tropical southeastern Indian Ocean. Mar Ecol Prog Ser 384:69–82

Saha S, Moorthi S, Pan H-L, Wu X, Wang J, Nadiga S, Tripp P, Kistler R, Woollen J, Behringer D, Liu H, Stokes D, Grumbine R, Gayno G, Wang J, Hou Y-T, Chuang H, Juang H-MH, Sela J, Iredell M, Treadon R, Kleist D, Delst PV, Keyser D, Derber J, Ek M, Meng J, Wei H, Yang R, Lord S, van den Dool H, Kumar A, Wang W, Long C, Chelliah M, Xue Y, Huang B, Schemm J-K, Ebisuzaki W, Lin R, Xie P, Chen M, Zhou S, Higgins W, Zou C-Z, Liu Q, Chen Y, Han Y, Cucurull L, Reynolds RW, Rutledge G, Goldberg M (2010) The NCEP climate forecast system reanalysis. Bull Am Meteorol Soc 91:1015–1057

Schlitzer R (2015) Ocean data view. http://odv.awi.de

Stroeve JC, Serree MC, Holland MM, Kay JE, Malanik J, Barrett AP (2012) The Arctic's rapidly shrinking sea ice cover: a research synthesis. Clim Change 110:1005–1027

Takahashi K (1987) Seasonal fluxes of silicoflagellates and *Actiniscus* in the subarctic Pacific during 1982–1984. J Mar Res 45: 397–425

Takahashi K, Billings JD, Morgan JK (1990) Oceanic province: assessment from the time-series diatom fluxes in the northeastern Pacific. Limnol Oceanogr 35:154–165

Takahashi K, Onodera J, Katsuki K (2009) Significant populations of seven-sided *Distephanus* (Silicoflagellata) in the sea-ice covered environment of the central Arctic Ocean, summer 2004. Micropaleontology 55:313–325

Vørs N (1992) Heterotrophic amoebae, flagellates, and heliozoa from the Tvärminne area, Gulf of Finland, in 1988–1990. Ophelia 36:1–109

Wang J, Hu H, Goes J, Miksis-Olds J, Mouw C, D'Sa E, Gomes H, Wang DR, Mizobata K, Saitoh S, Luo L (2013) A modeling study of seasonal variations of sea ice and plankton in the Bering and Chukchi Seas during 2007–2008. J Geophys Res Oceans 118:1–14. doi:10.1029/2012JC008322

Wassmann P, Duarte CM, Agust S, Sejr MK (2011) Footprints of climate change in the Arctic marine ecosystem. Glob Change Biol 17:1235–1249

Watanabe E, Kishi MJ, Ishida A, Aita MN (2012) Western Arctic primary productivity regulated by shelf-break warm eddies. J Oceanogr 68:703–718. doi:10.1007/s10872-012-0128-6

Watanabe E, Onodera J, Harada N, Honda MC, Kimoto K, Kikuchi T, Nishino S, Matsuno K, Yamaguchi A, Ishida A, Kishi MJ (2014) Enhanced role of eddies in the Arctic marine biological pump. Nat Commun 5:3950. doi:10.1038/ncomms4950

Zernova VV, Nöthig E-M, Shevchenko VP (2000) Vertical microalga flux in the northern Laptev Sea (from the data collected by the yearlong sediment trap). Oceanology 40:801–808